SYNTHESIS OF FULLERENES AND FULLERENIC NANOSTRUCTURES IN A LOW-PRESSURE BENZENE/OXYGEN DIFFUSION FLAME

PETER HEBGEN,[1] ANISH GOEL,[1] JACK B. HOWARD,[1] LENORE C. RAINEY[2] AND JOHN B. VANDER SANDE[2]

[1]*Department of Chemical Engineering*
[2]*Department of Material Science and Engineering*
Massachusetts Institute of Technology
77 Massachusetts Avenue
Cambridge, MA 02139, USA

Samples of condensable material from laminar low-pressure benzene/argon/oxygen diffusion flames were collected and analyzed by high-performance liquid chromatography to determine the yields of fullerenes and by high-resolution transmission electron microscopy (HRTEM) to characterize the fullerenic material (i.e., curved-layer nanostructures) on and within the soot particles. The highest concentration of fullerenes was always detected just above the visible stoichiometric surface of a flame. The percentage of fullerenes in the condensable material increases with decreasing pressure. The overall highest amount of fullerenes was found for a surprisingly high dilution of fuel with argon. A comparison of the flames with the same cold gas velocity of fuel and oxygen showed a strong dependence of fullerene content on flame length. A shorter flame, resulting from higher dilution or lower pressure, favors the formation of fullerenes rather than soot, and the amount of soot and precursors of both soot and fullerenes is less at lower pressure and higher dilution. This behavior indicates a stronger correlation of fullerene consumption to the total amount of soot than of fullerene formation to precursor concentration. The maximum flame temperature seems to be of minor importance in fullerene formation. The HRTEM analysis of the soot showed an increase of the curvature of the carbon layers, and hence increased fullerenic character, with increasing distance from the burner up to the point of maximum fullerene concentration. After this maximum, where soot and fullerenes are consumed by oxidation, the curvature decreases. In addition to the soot, the samples included fullerenic nanostructures such as tubes and spheroids including highly ordered multilayered or onionlike structures. The soot itself shows highly ordered regions that appear to have been cells of ongoing fullerenic nanostructure formation.

Introduction

Fullerenes, a new form of carbon, were discovered in 1985 [1] in graphite vaporization under inert gas at low pressure. Fullerenes have many properties different from either diamond or graphite. Potential applications include superconductors, sensors, catalysts, optical and electronic devices, polymer composites, high-energy fuels, and biological and medical materials. Other interesting classes of fullerenic or curved-layer carbon, as opposed to graphitic or planar-layer carbon, that can also be found in fullerene-producing systems are nanostructures with tubular, spheroidal, or other shapes and consisting of onionlike or nested closed shells [2–5] and soot particles with considerable curved-layer content [6,7].

Fullerenes can also be formed in premixed hydrocarbon flames under reduced-pressure and fuel-rich conditions. They were first detected in flames in ionic form by the Homann group [8,9] and later isolated in macroscopic quantities by Howard et al. [10–12]. Higher fullerenes [13], derivatives containing hydrogen and oxygen [14,15], and fullerenic nanostructures [4,5,16] and soot [6,7] have also been detected in premixed flames.

The highest yields of fullerenes in flames are obtained under conditions of substantial soot formation. To understand the mechanism of fullerene formation and enable the design of practical combustion systems for large-scale fullerene production, more information on fullerene yields under various conditions is needed. Little work has been reported on the formation of fullerenes in diffusion flames.

To explore the effects of pressure and diluent gas on fullerene yields in diffusion flames, samples of condensable material from diffusion flames under different conditions were collected and analyzed to determine the concentration of fullerenes, to
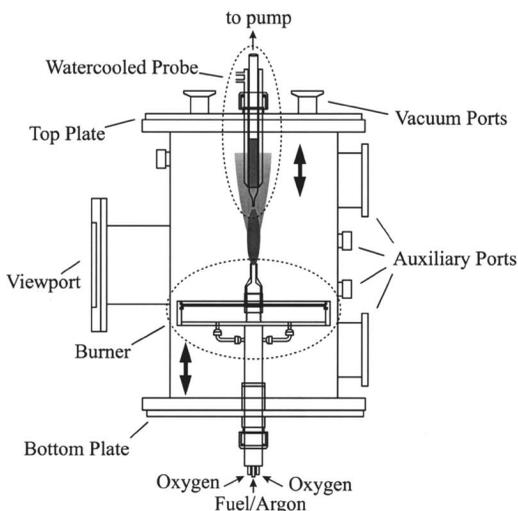
FIG. 1. Experimental setup.

identify fullerenic nanostructures, and to characterize the curvature of the carbon layers in the soot.

Experimental

The experimental setup for the burning of low-pressure laminar diffusion flames of benzene vapor diluted with argon in oxygen is shown in Fig. 1. The vertically adjustable burner consists of a 10 mm inside diameter (i.d.) fuel outlet tube surrounded by a 30.5 cm diameter porous bronze plate through which oxygen is fed.

The cold gas velocity of the unburned benzene/argon mixture, v_u(fuel/Ar), was 820 or 840 cm/s, and the dilution with argon, dil_{Ar}, was varied from 65% to 87.6%. Oxygen was kept at a cold gas velocity, v_u(oxy), of 3.65 cm/s. The pressure, p, in the burning chamber was varied from 12 to 40 torr.

A 10 mm i.d. vertically adjustable quartz microprobe with an orifice of 1.5–2 mm was used for sampling the flames. The probe was held in a water-cooled jacket and operated at ∼2 torr. Condensable combustion products including polycyclic aromatic hydrocarbons (PAH), fullerenes, and soot were collected on a preweighed filter system, consisting of a glass wool plug in an aluminum foil sleeve. Sampling times ranged from 1 to 5 minutes and were limited by soot clogging the probe. More heavily sooting conditions than those studied here could not be measured. The non-condensable gas from the filter was collected in a graduated water column. The mass of the filter was measured after sampling to determine the amount of flame material collected. The filter was then submerged in toluene and ultrasonicated, and the solution was filtered through a 0.45 μm nylon filter and analyzed for fullerenes with a high-performance liquid chromatograph (HPLC) (Cosmosil Buckprep column, 4.6 × 250 mm with 1.0 mL/min toluene) with a variable wavelength detector calibrated for C_{60} and C_{70}, using a wavelength of 330 nm.

Samples from different heights above the burner in the axial center of the flame were taken by changing the vertical positions of the burner and the probe. The ratios of the total mass of fullerenes to the total mass of condensable material and to the total volume of the noncondensable gas were used as parameters to characterize the fullerene production in the flames.

The maximum flame temperatures were determined with a calibrated pyrometer (Micro Optical Pyrometer 95C, Pyrometer Instrument Co., Inc.) and corrected for a spectral emissivity of 0.85, which gave an addition of ∼20 K. Thermocouple pyrometry was not possible because of heavy soot deposition on the thermocouples in less than a second.

Soot particles and carbon nanostructures, including nanotubes and onionlike structures were analyzed by high-resolution transmission electron microscopy (HRTEM). A small amount of the sonicated toluene mixture was diluted with additional toluene and again ultrasonicated. A few drops of the diluted mixture were deposited on an electron microscope grid, and the toluene was allowed to evaporate prior to analysis. The grids consisted of a 200 mesh copper substrate on which a holey carbon film and a supporting polymeric substrate were deposited. The electron microscopes were operated at 200 keV with resolutions better than 0.2 nm. The curvatures, arc lengths, and diameters of carbon structures seen in the soot images were then quantified using a MatLab analysis tool described elsewhere [6].

Results

Fullerenes

The parameters of the flames studied are listed in Table 1. The HPLC analysis shows primarily C_{60} and C_{70} with small amounts of PAH, oxidized fullerenes, and higher fullerenes up to C_{96}. In all cases, C_{60} and C_{70} constitute over 95% of the mass of fullerenes analyzed by the chromatograph. Consequently, for data comparison, we used the mass of C_{60} and C_{70} relative to the total mass of condensable material as representative of the concentration of fullerenes. Table 1 shows the distance, h_{max}, from the fuel outlet to the probe inlet for the samples with the maximum percentage of fullerenes in the condensable material. Also shown are the maximum percentage of C_{60} and C_{70}, the maximum flame temperature, and the flame reference number used in later graphs.

TABLE 1
Flame parameters

p (torr)	v_u(fuel/Ar) (cm/s)	dil_{Ar} (% Ar)	v_u(oxy) (cm/s)	h_{max} (mm)	$C_{60} + C_{70}$ (mass %)	T_{max} (K)	Flame (Ref. #)
20	840	66.5	3.65	84.5	2.97	1659	5
20	840	71.0	3.65	74.5	6.83	1689	4
20	840	76.0	3.65	61.5	5.13	1635	3
40	820	80.3	3.65	96.5	3.15	1694	10
40	820	82.8	3.65	88	3.73	1726	8
40	820	85.3	3.65	74	4.49	1754	11
40	820	87.6	3.65	69	4.86	1694	12
12	820	65.0	3.65	57	12.44	1599	13
12	820	67.5	3.65	53	12.40	1583	14

The highest soot concentration in diffusion flames is in the wings of a flame, where the radial fuel and oxygen concentration gradients are highest and the temperature is maximum. Further from the flame axis, the soot is consumed by oxidation. The flame wings collapse to one point at the tip of the stoichiometric surface, where the flame reaches its highest overall temperature; therefore, the axial concentration gradients of fuel, oxygen, and products including soot are similar to the radial gradients closer to the burner.

Results from three 20 torr flames with different argon dilutions are shown in Fig. 2a and 2b. The amount of C_{60} and C_{70} as a mass percentage of the condensables is shown in Fig. 2a, and the concentration of C_{60} and C_{70} in the cold sampled gas is shown in Fig. 2b, both versus the height above the burner.

The highest concentration of fullerenes always occurred just above the visible stoichiometric surface of the flame, where the temperature maximum also occurs. Therefore, the locations of the maxima of the curves are indicative of the stoichiometric flame length. From Fig. 2a and 2b and Table 1, diluting the benzene with argon results in a shorter flame but not necessarily in a lower temperature, and a higher fullerene percentage does not necessarily indicate a higher fullerene concentration. A decrease in the concentration of condensable material can be large enough to offset the increase in fullerene percentage. Estimation of the percentage of the carbon fed that is converted into fullerenes from the flame #4 data gives 0.5%. This value, for non-optimized conditions, is comparable to the largest value observed in premixed benzene flames [11,12].

Data for flames at 40 torr (Fig. 2c and 2d) compared with those for 20 torr (Fig. 2a and 2b) show that increasing pressure increases the flame length while decreasing the flame diameter, resulting in a more heavily sooting flame. In general, the percentage of fullerenes is lower at 40 torr than at 20 torr.

For lower dilutions than those shown in Fig. 2c and 2d, large soot concentrations at 40 torr caused rapid probe clogging. With increasing dilution, the 40 torr flames show an increase in the maximum percentage of fullerenes (Fig. 2c) and a decrease in the maximum fullerene concentration (Fig. 2d). Although measurements were taken at dilutions up to 87.6%, where the temperature is lower than that of the next lower dilution, the peak in percentage of fullerenes is still higher. At lower dilutions, the concentration would be expected to decrease with decreasing dilution because the flame temperature goes down due to increased soot radiation. Such behavior is seen in premixed flames [11,12], where the concentration of fullerenes decreases with decreasing fuel dilution over a specified range of dilutions.

Two flames were studied at 12 torr (Table 1). Consistent with the other results, the flames were shorter and the percentage of the fullerenes was higher than at 20 torr.

The maximum percentage of fullerenes in the condensable material from the different flames decreases with increasing flame length in a strong relation, as shown in Fig. 2e. Shorter flames, which result from higher dilution or lower pressure, favor fullerenes over soot, possibly indicating fullerene consumption by soot, as has also been suggested based on behavior seen in premixed flames [17]. This consumption should be slower for lower pressures and higher dilutions because of lower soot concentrations. The effect of a lower precursor concentration seems to be overwhelmed.

For each set of flames at different pressures, the mass ratio of C_{60} to C_{70} at the maximum fullerene concentration for each flame increases with increasing dilution (Fig. 2f). However, unlike the fullerene percentage trend, this effect is pressure dependent.

Soot Structure Evolution

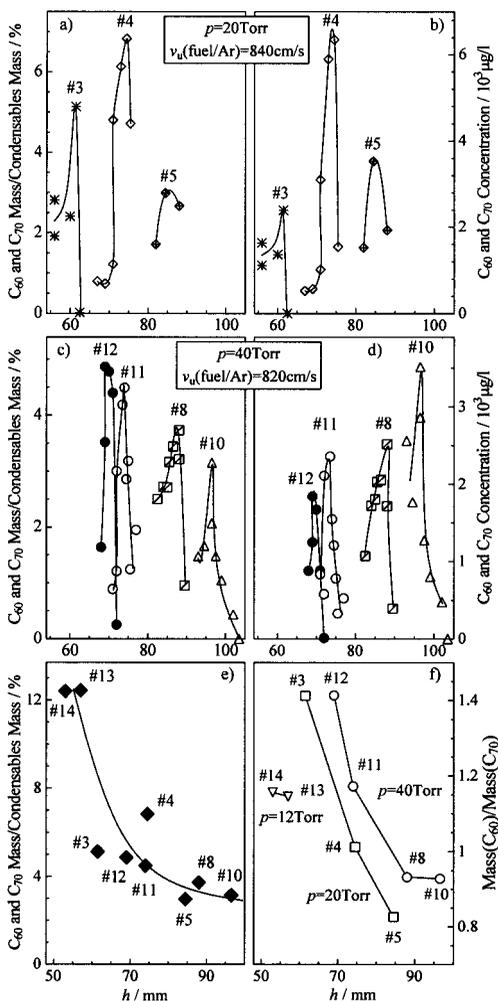An example of an HRTEM micrograph of soot from flame #11 (75 mm) is shown in Fig. 3 (the white

FIG. 2. Quantity of fullerenes C_{60} and C_{70} in the condensable material (a, c) and concentration of fullerenes C_{60} and C_{70} in the cold probed gas (b, d) from different heights above the burner in different flames and maximum amount of fullerenes C_{60} and C_{70} (e) and mass ratio of C_{60} to C_{70} (f) in the condensable material at the height above the burner corresponding to maximum fullerene concentration in flames, at different pressures (p) and different argon dilutions (dil_{Ar}).

FIG. 3. Representative HRTEM image of condensable material collected at $h = 75$ mm in flame #11 ($p = 40$ torr, v_u(fuel/Ar) = 820 cm/s, v_u(oxy) = 3.65 cm/s, dil_{Ar} = 85.3%).

FIG. 4. Representative counted material from soot collected at $h = 72$ mm (a), 74 mm (b), 75 mm (c), and 77 mm (d) in flame #11 ($p = 40$ torr, v_u(fuel/Ar) = 820 cm/ s, v_u(oxy) = 3.65 cm/s, dil_{Ar} = 85.3%).

color in the images represents carbon layers or shells). The inset shows an enlarged area with closed shells. Significantly more ordered and more curved carbon layers or shells were seen in this study than in premixed benzene combustion [6].

Figure 4 shows soot from four different heights above the burner that were used for the curvature analysis. Carbon structures along the periphery of
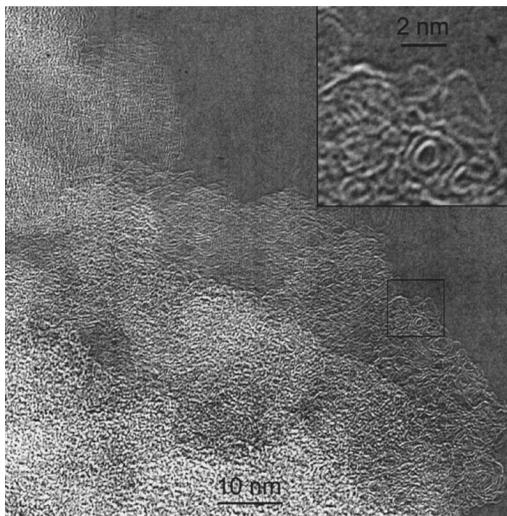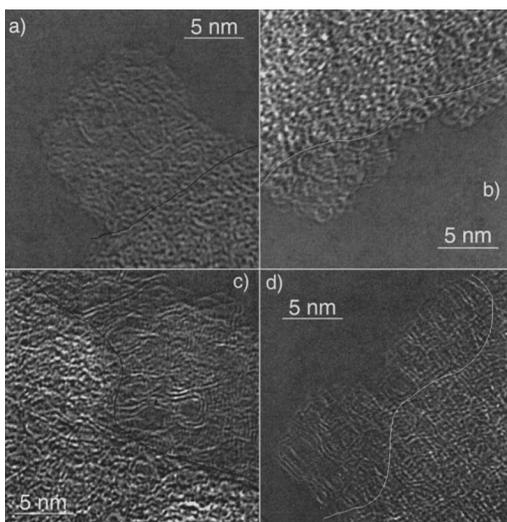
the soot particles were analyzed quantitatively to determine the evolution of the structures with increasing height above the burner. Only the periphery of the particles was thin enough to allow for accurate measurements of the layers. The hand-drawn lines show the boundary between the outside area that was counted and the particle interior.
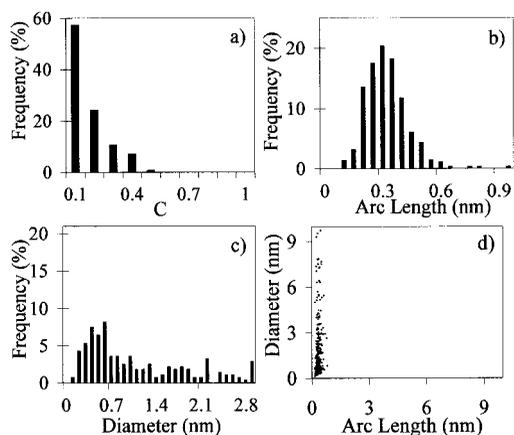
FIG. 5. Normalized histograms of curvature (a), arc length (b), and diameter (c) and arc length versus diameter scatter plot (d) of amorphous carbon material.
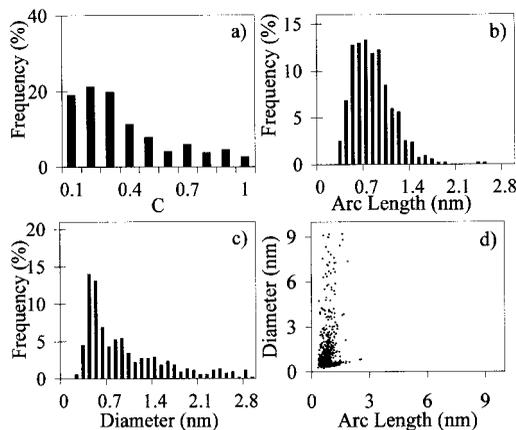

FIG. 6. Normalized histograms of curvature (a), arc length (b), and diameter (c) and arc length versus diameter scatter plot (d) of condensable material collected at h = 72 mm in flame #11 (p = 40 torr, v_u(fuel/Ar) = 820 cm/s, v_u(oxy) = 3.65 cm/s, dil_{Ar} = 85.3%).

FIG. 7. Normalized histograms of curvature (a), arc length (b), and diameter (c) and arc length versus diameter scatter plot (d) of condensable material collected at h = 74 mm in flame #11 (p = 40 torr, v_u(fuel/Ar) = 820 cm/s, v_u(oxy) = 3.65 cm/s, dil_{Ar} = 85.3%).

FIG. 8. Normalized histograms of curvature (a), arc length (b), and diameter (c) and arc length versus diameter scatter plot (d) of condensable material collected at h = 75 mm in flame #11 (p = 40 torr, v_u(fuel/Ar) = 820 cm/s, v_u(oxy) = 3.65 cm/s, dil_{Ar} = 85.3%).

Two properties of the curved layers or shells, arc length (L) and diameter (D), were measured directly and used to calculate a non-dimensional parameter, curvature ($C = L/\pi D$). Values of C range from 0 for a graphitic sheet to unity for a closed shell. Normalized histograms of each of these parameters and scatter plots of arc length versus diameter are shown for each of the four samples and amorphous carbon in Figs. 5–9. The truncation of the x axes in these figures causes some of the histograms to sum to less than 100.

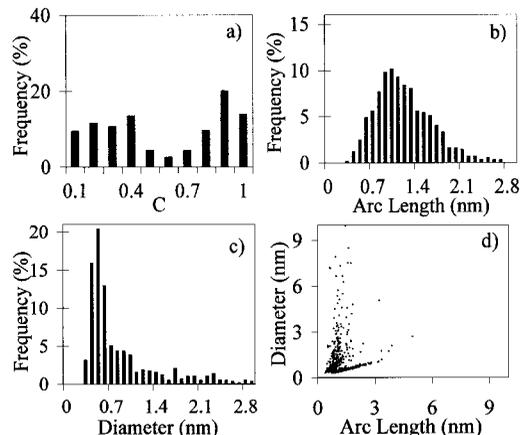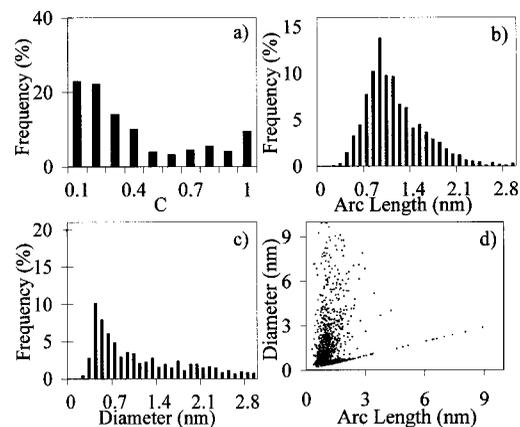It can be seen that the structures in this amorphous carbon sample, compared with those of any

flame sample, have very low curvatures and are relatively short. The large diameters seen in the amorphous carbon are due to the relatively flat nature of the structures. As a consequence of the analysis method, the flatter of two structures with equal arc length will have a greater measured diameter.

A comparison of the curvature histograms in Figs. 5–9 (parts a) shows that curvature increases with distance until the fullerene maximum (74 mm), where it then decreases. This indicates that the observed fullerene peak is also the peak for the generation of completely closed-shell structures. The histograms
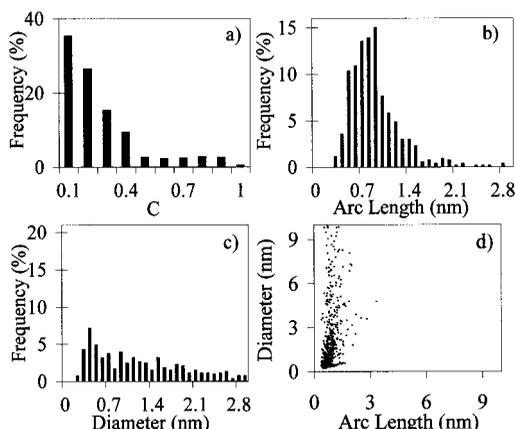
FIG. 9. Normalized histograms of curvature (a), arc length (b), and diameter (c) and arc length versus diameter scatter plot (d) of condensable material collected at $h = 77$ mm in flame #11 ($p = 40$ torr, v_u(fuel/Ar) $= 820$ cm/s, v_u(oxy) $= 3.65$ cm/s, $dil_{Ar} = 85.3\%$).
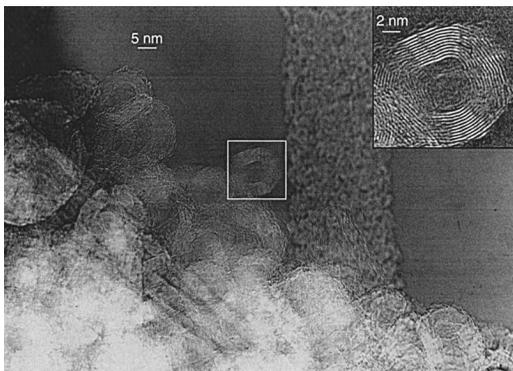

FIG. 10. HRTEM image of fullerenic nanostructures in condensable material collected at $h = 61$ mm in flame #13 ($p = 12$ torr, v_u(fuel/Ar) $= 820$ cm/s, v_u(oxy) $= 3.65$ cm/s, $dil_{Ar} = 65.0\%$).

in parts b of the figures show a similar behavior in that arc lengths increase until a dropoff is observed after the fullerene maximum. The part c histograms show a decrease in diameter with increasing distance until the fullerene maximum, followed by an increase. The diameter peak is seen at 0.7 nm, the diameter of a C_{60} molecule, and highest at 74 mm, then becoming less pronounced after the fullerene maximum. In the scatter plots of parts d, points that lie on the delineated lower boundary represent complete closed-shell structures. It appears that larger closed-shell structures are more prevalent with increasing distance until they practically disappear at 77 mm. Considering these trends collectively, it can

be seen that the carbon structures in the soot become more curved and more closed until the fullerene peak, then change to flatter, smaller structures.

The sample images were examined qualitatively for the emergence of fullerenic nanostructures. Fig. 10 shows a micrograph representative of the nanostructures from flame #13 at 61 mm, which consist of stacked layers of apparently fullerenic carbon and include nanotubes and highly ordered onionlike structures. The inset in Fig. 10 shows an enlarged onionlike closed-shell nanostructure. Similar structures have been seen in fullerene-forming premixed benzene flames [6,14–16].

Discussion

Fullerenes

The elimination of CO from oxidized PAH is thought to be a source of five-membered rings [18] in the structure of combustion-generated PAH, which are precursors to fullerenes in flames [19–21]. However, the highest concentration of fullerenes is in the region of the flame where the precursor concentration is decreasing due to oxidation. Oxidation reactions are also responsible for the decomposition of the fullerenes at greater distances.

That the maximum fullerene percentage is at such high fuel dilutions as those seen here may indicate that fullerene consumption by soot is important. At 40 torr (Fig. 2c and 2d), the percentage of fullerenes is highest at the highest dilution, but the temperature is lower compared with lower dilutions. The overall carbon concentration in the flame and soot formation decrease with increasing dilution. The lower soot concentrations at higher dilutions reduce radiative heat loss from the flame, partially offsetting the lower heat production due to less fuel. At the same time, the concentration of precursors for fullerenes, as well as soot, is decreasing, but the flames with the lowest total concentration exhibit the highest fullerene percentage. Similarly, decreasing pressure lowers total soot and fullerene concentration but still raises the percentage of fullerenes. Associated with these effects is the observed strong correlation in which shorter flames yield higher percentages of fullerenes in the condensable material.

Although this provides a qualitative explanation for the appearance of a maximum rate of fullerene formation, a quantitative prediction for the optimal dilution is not yet possible. It is possible, however, to vary the percentage of fullerenes in the soot and the distribution between the fullerenes over a wide range by varying pressure, dilution, and cold gas velocity in the right combination.

Soot Structure Evolution

The electron microscope images show a soot microstructure that is different from samples collected

from higher-pressure flames as well as low-pressure premixed flames [6]. Structures similar to those seen here have also been found in commercially produced carbon black [22,23]. Quantitative analysis of the micrographs using the curvature parameter cited above indicates that carbon layers or shells in the soot become more curved (i.e., more fullerenic) with increasing distance in the flame up to the fullerene maximum, after which the curvature declines (Figs. 5–9). The arc length increases with distance, indicating growth to larger structures, while diameter decreases, indicating increase of curvature of layers already present in the soot or addition to the soot of smaller-diameter fullerenic carbon. Together, these trends indicate that gas-phase-formed fullerenes are consumed by, and presumably incorporated into, the soot and nanostructures. This behavior is consistent with the hypothesis that fullerenes added to the soot from the gas phase are a source of the fullerenic structures, including closed shells, of around 0.7 nm diameter seen in the soot micrographs. The added fullerenes might also contribute, along with other polycyclic material in the soot, to the growth of larger curved layers indicated by the increase of arc length. The correspondence of the diminishing of the 0.7 nm diameter peak and the fullerene maximum is also consistent with the fullerene-addition hypothesis.

The quantity of nanotubes and onionlike structures (Fig. 10) is higher than in premixed flames [6], where nanostructures are seen only at long residence times after oxygen depletion. In our flames, nanostructures appear soon after the stoichiometric flame surface where the maximum temperature occurs and the fullerenes and soot are being oxidized. Consequently, the timescale for nanostructure formation in diffusion flames must be shorter than that for premixed combustion. We conclude that fullerenic nanostructures are formed after the fullerene peak where soot and fullerenes are being consumed by oxidation. The images appear to show nanostructure precursors that were being formed from the soot material.

Summary

The evolution of fullerenes, fullerenic soot material, and fullerenic nanostructures with increasing distance from the fuel outlet, as concluded by the findings in this study, can be summarized as follows:

- Prior to stoichiometric surface: pre-C_{60} incubation, presence of relatively flat soot structures, and curvature of soot structures and concentration of C_{60}/C_{70} increasing with distance
- Just above stoichiometric surface: peak of C_{60}/C_{70} concentration, maximum temperature and soot structure curvature, and presence of nanostructure precursor cells
- After stoichiometric surface: fullerenes consumed by oxidation and incorporation into nanostructures, curvature of soot structures and concentration of C_{60}/C_{70} decreasing with distance, and appearance of fullerenic nanostructures

REFERENCES

1. Kroto, H. W., Heath, J. R., O'Brien, S. C., Curl, R. E., and Smalley, R. E., *Nature* 318:162 (1985).
2. Iijima, S., *Nature* 354:56 (1991).
3. Ugarte, D., *Carbon* 33:989 (1995).
4. Howard, J. B., Chowdhury, K. D., and Vander Sande, J. B., *Nature* 370:603 (1994).
5. Chowdhury, K. D., Howard, J. B., and Vander Sande, J. B., *J. Mater. Res.* 11:341 (1996).
6. Grieco, W. J., Howard, J. B., Rainey, L. C., Vander Sande, J. B., *Carbon* 38:597 (2000).
7. Werner, H., Herein, D., Blöcker, J., Henschke, B., Tegtmeyer, U., Schedelniedrig, T., Keil, M., Bradshaw, A. M., and Schlogl, R., *Chem. Phys. Lett.* 194:62 (1992).
8. Gerhardt, P., Löffler, S., and Homann, K.-H., *Chem. Phys. Lett.* 137:306–310 (1987).
9. Gerhardt, P., Löffler, S., and Homann, K.-H., *Proc. Combust. Inst.* 22:395 (1989).
10. Howard, J. B., McKinnon, J. T., Makarovsky, Y., Lafleur, A. L., and Johnson, M. E., *Nature* 352:139 (1991).
11. Howard, J. B., McKinnon, J. T., Johnson, M. E., Makarovsky, Y., and Lafleur, A. L., *J. Phys. Chem.* 96:6657 (1992).
12. Howard, J. B., Lafleur, A. L., Makarovsky, Y., Mitra, S., Pope, C. J., and Yadav, T. K., *Carbon* 30:1183 (1992).
13. Richter, H., Labrocca, A. J., Grieco, W. J., Taghizadeh, K., Lafleur, A. L., and Howard, J. B., *J. Phys. Chem. B* 101:1556 (1997).
14. Anacleto, J. F., Boyd, R. K., Pleasance, S., Quilliam, M. A., Howard, J. B., Lalfeur, A. L., and Makarovsky, Y., *Can. J. Chem.* 70:2558 (1992).
15. Anacleto, J. F., Quilliam, M. A., Boyd, R. K., Howard, J. B., Lalfeur, A. L., and Yadav, T. K., *Rapid Communication in Mass Spectrometry* 7:229 (1993).
16. Richter, H., Hernadi, K., Cauano, R., Fonseca, A.,

Migeon, H.-N., Nagy, J. B., Schneider, S., Vandooren, J., and Van Tiggelen, P. J., *Carbon* 34:427 (1996).

17. Grieco, W. J., Lafleur, A. L., Swallow, K. C., Richter, H., Taghizadeh, K., and Howard, J. B., *Proc. Combust. Inst.* 27:1669 (1998).

18. Bittner, J. D., and Howard, J. B., *Proc. Combust. Inst.* 18:1105 (1981).

19. Ahrens, J., Bachmann, M., Baum, T., Griesheimer, J., Kovacs, R., Weilmünster, P., and Homann, K.-H., *Int. J. Mass Spectrom. Ion Processes* 138:133 (1994).

20. Pope, C. J., Marr, J. A., and Howard, J. B., *J. Phys. Chem.* 97:11001 (1993).

21. Lafleur, A. L., Howard, J. B., Marr, J. A., and Yadav, T., *J. Phys. Chem.* 97:13539 (1993).

22. Donnet, J. B., *Rubber Chem. Technol.* 71:323 (1998).

23. Donnet, J. B., Wang, T. K., Wang, C. C., Monthioux, M., Johnson, M. P., Norman, D. T., Wansborough, R. W., and Bertrand, P., *KGK Kautschuk Gummi Kunststoffe,* Hüthig GmbH, Hiedelberg, Germany, 1999, p. 340.

COMMENTS

Albert Wagner, Argonne National Laboratory, USA. Is there any point in the flame where there is a substantial amount of fullerenes but no condensed soot particles?

Author's Reply. At larger distances from the burner than those for which data are shown in Fig. 2, the mass ratio of fullerenes to soot increases, and visual observation indicates the absence of soot. However, probe sampling with filter analysis yields collected soot. We have never observed fullerenes without soot in samples from diffusion flames. We have observed fullerenes in the absence of soot in samples collected from an almost but not quite sooting premixed benzene/oxygen flame (C/O = 0.72) at a pressure of 20 Torr (Ref. [11] in this paper).

●

Paul Roth, University of Duisburg, Germany. What is the influence of particle probing from the flame and probe after treatment on the carbon structures you were showing?

Author's Reply. From our previous studies of the formation of fullerenic carbon structures in premixed flames, where the time resolution is much better than in the present diffusion flames, we know that the timescale for the structural changes observed here is much larger than the timescale for quenching in the probe. Therefore, it is safe to assume that the structure of the sample material is essentially the same as the structure of the material in the flame at the location sampled.

●

Alexander Fridman, University of Illinois at Chicago, USA. Calculating arc length as a function of diameter, the fullerene-like structures were considered as complete circles. It would be interesting to consider their shape in more detail. This would give information on the relation between the fullerenes in the gas phase and the corresponding structures in soot.

Author's Reply. It would be interesting to do a more sophisticated structure analysis of the single structures and also to analyze the interstructure characteristics, which may be possible with the diffraction pattern analysis that we are currently developing.

●

R. A. Dobbins, Brown University, USA. Can you comment on the relative production rate/efficiency of fullerenes in diffusion flames versus premixed flames?

Author's Reply. For non-optimized diffusion flame conditions, we are in the same relative production range that we achieved with premixed flames. We are currently studying both premixed and diffusion flames in more detail and over wider ranges of the most important conditions.